Quantum Quench and Nonequilibrium Dynamics in Lattice-Confined Spinor Condensates

Z. Chen, T. Tang, J. Austin, Z. Shaw, L. Zhao, and Y. Liu*
Department of Physics, Oklahoma State University, Stillwater, Oklahoma 74078, USA

(Received 20 May 2019; published 10 September 2019)

We present an experimental study on nonequilibrium dynamics of a spinor condensate after it is quenched across a superfluid to Mott insulator (MI) phase transition in cubic lattices. Intricate dynamics consisting of spin-mixing oscillations at multiple frequencies are observed in time evolutions of the spinor condensate localized in deep lattices after the quantum quench. Similar spin dynamics also appear after spinor gases in the MI phase are suddenly moved away from their ground states via quenching magnetic fields. We confirm these observed spectra of spin-mixing dynamics can be utilized to reveal atom number distributions of an inhomogeneous system, and to study transitions from two-body to many-body dynamics. Our data also imply the nonequilibrium dynamics depend weakly on the quench speed but strongly on the lattice potential. This enables precise measurements of the spin-dependent interaction, a key parameter determining the spinor physics.

DOI: 10.1103/PhysRevLett.123.113002

Spinor Bose-Einstein condensates (BECs) are multicomponent condensates possessing a spin degree of freedom [1]. Combined with optical lattices and microwave dressing fields, spinor gases offer an unprecedented degree of control over many parameters and have thus been considered as ideal candidates for studying nonequilibrium dynamics [1–12]. Such a system can be easily prepared far away from equilibrium through quenching one of its highly controllable parameters, e.g., the number of atoms, temperature, total spin of the system, the lattice potential, or the dimensionality of the system [1–10]. Interesting dynamics have also been initiated in lattice-confined spinor gases by nonequilibrium initial states, such as interaction-driven revival dynamics in one-dimensional Ising spin chains [13], dynamics and equilibration of spinor BECs in two-dimensional lattices [3], and spin-mixing dynamics of tightly confined atom pairs in cubic lattices [14,15]. Another notable advantage of spinor systems on investigating nonequilibrium dynamics is their long equilibration time, ranging from tens of milliseconds to several seconds [1,3]. Experimental studies on nonequilibrium dynamics have been conducted in spinor gases extensively at two extremes, i.e., in a clean two-body system with a pair of atoms in the Mott-insulator (MI) phase [14,15], and in a many-body system with more than 10^4 atoms in the superfluid (SF) phase [1–4]. Transitions between these two extremes, however, remain less explored [5].

In this Letter, we experimentally confirm that lattice-trapped spinor BECs provide a perfect platform to understand these less-explored transitions. Our experiments are performed in a quantum quench scenario starting with an antiferromagnetic spinor BEC at its SF ground state, based on a theoretical proposal in Ref. [5]. We continuously quench the potential of a cubic lattice to a very large value, completely suppressing tunnelings to freeze atom number distributions in individual lattice sites. Spin dynamics are observed at fast quench speeds, and adiabatic SF-MI quantum phase transitions are detected after sufficiently slow lattice ramps. About half of the data shown in this Letter are collected after the lattice is quenched at an intermediate speed, which is slow enough to prevent excitations to higher vibrational bands while remaining fast enough to suppress hopping among lattice sites. We observe dynamics consisting of spin-mixing oscillations at multiple frequencies in spinor BECs after the quantum quench in magnetic fields of strength $B < 60\ \mu$T. The remaining data are taken after adiabatic lattice ramps. Similar spin dynamics also occur after we abruptly move spinor gases in the MI phase away from their ground states via quenching magnetic fields. In our system, an inhomogeneous system with an adjustable peak occupation number per lattice site (n_{peak}), a significant amount of lattice sites are occupied by more than two atoms. The observed spin-mixing spectra are thus utilized to study transitions between two-body and many-body spin dynamics and to reveal atom number distributions of an inhomogeneous system. Our data also indicate the nonequilibrium dynamics depend weakly on the quench speed but strongly on the lattice potential. We find every observed spin dynamics is well described by a sum of multiple Rabi-type spin-mixing oscillations. This enables us to precisely measure the ratio of the spin-independent interaction U_0 to the spin-dependent interaction U_2, an important factor determining the spinor physics.

The site-independent Bose-Hubbard model has successfully described lattice-confined spinor BECs [5,16,17]. We can understand our data taken in deep lattices with a simplified Bose-Hubbard model by ignoring the tunneling energy J as follows [5,17]:

$$H=\frac{U_0}{2}n(n-1)+\frac{U_2}{2}(\vec{S}^2-2n)+q(n_1+n_{-1})-\mu n. \quad (1)$$

Here, q is the net quadratic Zeeman energy induced by magnetic and microwave fields, μ is the chemical potential, $n=\sum_{m_F} n_{m_F}$ is the total atom number in each lattice site with n_{m_F} atoms staying in the hyperfine m_F state, and $\vec{S}$ is the spin operator [5,17].

We start each experimental cycle at $q/h=40$ Hz in free space with a spin-1 antiferromagnetic spinor BEC of up to 10^5 sodium atoms in its ground state, the longitudinal polar (LP) state with $\rho_0=1$ and $m=0$ [18]. Here ρ_{m_F} is the fractional population of the m_F state, $m=\rho_{+1}-\rho_{-1}$ is the magnetization, and h is the Planck constant. Two different quench sequences, Quench-L and Quench-Q, are applied in this Letter [18]. In the Quench-L sequences, we tune magnetic fields to a desired q and then quench up the depth u_L of a cubic lattice from 0 to $28(2)E_R$ within a time duration $t_{\rm ramp}$, where E_R is the recoil energy [18]. This final depth u_L is much larger than SF-MI transition points and thus deep enough to localize atoms into individual lattice sites. In the Quench-Q sequences, we adiabatically ramp up cubic lattices to a final depth of $u_L\geq 28E_R$ in a high field (where $q\gg U_2$), which ensures atoms cross SF-MI transitions and enter into their ground states (where $\rho_0\simeq 1$) in the MI phase [16], and we then suddenly quench magnetic fields to a desired q for initiating nonequilibrium dynamics. After each quench sequence, we hold atoms in lattices for a certain time $t_{\rm hold}$, then measure ρ_0 based on Ref. [18].

Nonequilibrium dynamics consisting of spin-mixing oscillations at multiple frequencies are observed after both Quench-L and Quench-Q sequences in spinor gases localized in deep lattices at $q/h<100$ Hz. Two typical time evolutions detected after Quench-Q sequences are shown in Fig. 1(a). Such an evolution appears to be fit by a composition of multiple Rabi-type oscillations [see solid lines in Fig. 1(a) and Eq. (2)]. This can be explained by considering that n atoms tightly confined in one lattice site display a Rabi-type oscillation at a fixed frequency f_n, and the observed dynamics combine all time evolutions occurring in individual lattice sites for our inhomogeneous system. We derive $f_n=E_n/h$ from Eq. (1), where E_n is the energy gap between the ground state and the first excited state in the subspace of $m=0$ at a given n [see Fig. 1(b)]. Analytical expressions for f_n can be found at $n=2$ and $n=3$, i.e., $f_2=U_2\sqrt{9-4(q/U_2)+4(q/U_2)^2}/h$ and $f_3=U_2\sqrt{25+4(q/U_2)+4(q/U_2)^2}/h$. We develop the following empirical formula based on the predicted f_n for an inhomogeneous system with a certain $n_{\rm peak}$, and find all

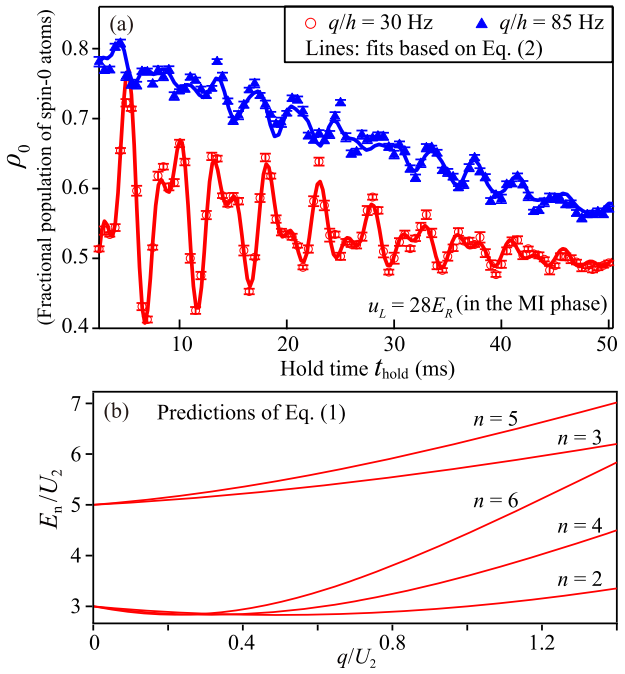

FIG. 1. (a) Observed spin dynamics after Quench-Q sequences to different q. Lines are fits based on Eq. (2) [18]. (b) Lines denote the predicted energy $E_n=hf_n$ (see text).

observed spin dynamics can be fit by this formula [see typical examples in Fig. 1(a) and Ref. [18]],

$$\rho_0(t)=\sum_{n=2}^{n_{\rm peak}}A_n\exp(-t/\tau_n)\sin[2\pi f_n(t-t_0)] + \Delta\rho_0\exp(-t/\tau_0)+\frac{1}{3}. \quad (2)$$

Here, the first term combines individual Rabi-type oscillations at all possible n with $1/\tau_n$ being the damp rate for oscillation amplitudes and t_0 marking the beginning of oscillations, while the second term describes an overall decay of spin oscillations at a decay rate of $1/\tau_0$. This decay may be mainly due to unavoidable lattice-induced heatings. The third term of Eq. (2) indicates the three spin components equally distribute in equilibrium states when $t_{\rm hold}\to\infty$ [3,19]. The validity of Eq. (2), a conservative model, may be justified by the fact that observed atom losses are less than 10% within every time evolution studied in this Letter.

To better illustrate the spin-mixing dynamics, we conduct fast Fourier transformations (FFT) onto all observed time evolutions. Two typical FFT spectra extracted from the same dataset over different time durations are shown in Fig. 2(a), where the vertical lines mark the five f_n predicted by Eq. (1). Each of these two FFT spectra has five distinguished peaks agreeing well with the predictions of Eq. (1); i.e., all spin components in the three even Mott lobes oscillate at lower frequencies while particles in the two odd Mott lobes display higher spin oscillation

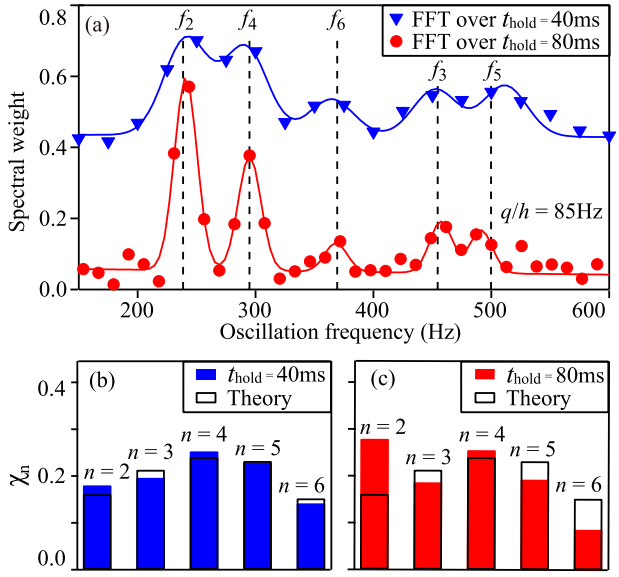

FIG. 2. (a) Triangles (circles) represent fast Fourier transformations (FFT) over the first 40 ms (80 ms) of $t_{\rm hold}$ on the $q/h = 85$ Hz dataset shown in Fig. 1(a). Vertical lines mark the predicted f_n (see text). Solid lines are five-Gaussian fits. Results obtained at $t_{\rm hold} = 40$ ms are shifted up by 0.4 for visual clarity. (b) Atom number distributions extracted from the $t_{\rm hold} = 40$ ms FFT spectrum in panel (a). We define χ_n as the fraction of atoms localized in lattice sites having n atoms, and extract χ_n from dividing the area below the corresponding peak in a FFT spectrum by the spin oscillation amplitude D_n (see Ref. [20]). Black bars mark the predicted χ_n in Mott-insulator shells at $n_{\rm peak} = 6$ based on Eq. (1) and the Thomas-Fermi approximation. (c) Similar to panel (b) but extracted from the $t_{\rm hold} = 80$ ms FFT spectrum in panel (a).

frequencies when $q/U_2 < 1.55$. Atom number distributions in the spinor gases can also be revealed from the corresponding FFT spectrum over a given time duration, as explained in Figs. 2(b) and 2(c). A comparison between these two figures clearly demonstrates that number distributions χ_n in our system quickly change with time $t_{\rm hold}$ and the $n = 2$ Mott lobe becomes more dominating after atoms are held in deep lattices for a longer time. This implies atoms in the $n = 2$ Mott lobe decay more slowly, which may be owing to a lack of three-body inelastic collisions in this lobe. Figure 2(b) shows another notable result: each experimental χ_n extracted from the FFT spectrum over a short time duration (i.e., $t_{\rm hold} = 40$ ms) coincides with the theoretical χ_n derived from Eq. (1) and the Thomas-Fermi approximation for Mott-insulator shells at $n_{\rm peak} = 6$. Atoms in initial states distribute into these predicted Mott shells during the Quench-Q sequences, because the initial states are the ground states of the MI phase. Our data thus experimentally confirm that the spin-mixing dynamics and their corresponding FFT spectra over a short $t_{\rm hold}$ can efficiently probe the initial Fock-state distributions after a sufficiently fast quench.

Similar nonequilibrium dynamics are also detected in time evolutions of spinor gases after Quench-L sequences under a wide range of magnetic fields (see Fig. 3). To our knowledge, this may be the first experimental observation of such complicated spin-mixing dynamics, although its theoretical model has been studied by Ref. [5]. Our observations indicate the spin-mixing dynamics weakly depend on $t_{\rm ramp}$ [21]. Typical examples can be seen in Fig. 3(a), where the data sets collected at distinct $t_{\rm ramp}$ display similar dynamics with almost identical oscillation frequencies and slightly different oscillation amplitudes. This may be due to the fact that $t_{\rm ramp}$ in a Quench-L sequence is carefully chosen for limiting all spin components to oscillate between the ground states and the first excited states.

The spin oscillations observed after Quench-L sequences can also be well fit by Eq. (2) [see Fig. 3(a)]. We can extract the spin-dependent interaction U_2 from these fitting curves, because U_2 decides frequency f_n when $n \geq 2$ at a fixed q. Figures 3(b) and 3(c) show 20 experimental values of U_2 extracted from our data taken under very different conditions. By applying linear fits to these data points, we find a precise value for two key parameters that determine the spinor physics, i.e., $U_2/U_0 \simeq 0.035(3)$ and $a_2/a_0 \simeq 1.115(10)$ for ^{23}Na atoms. Here a_2 and a_0 are s-wave scattering lengths, and $a_2/a_0 = (U_2 + U_0)/(U_0 - 2U_2)$ based on Refs. [25,26]. Many published values of

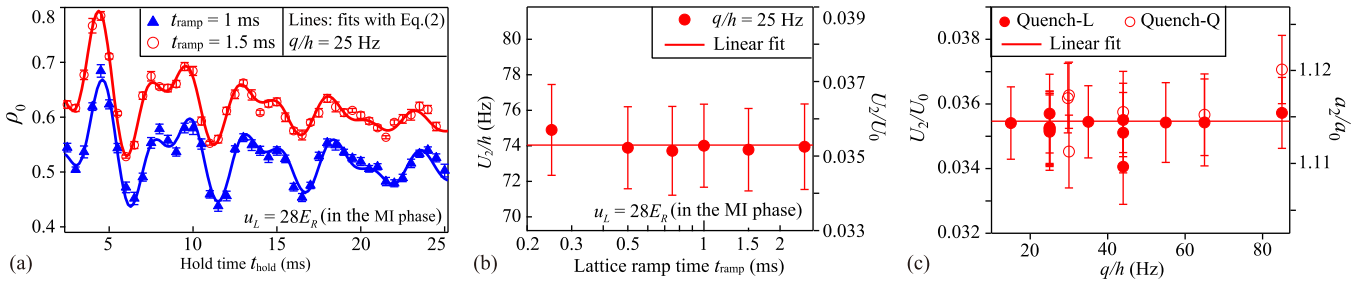

FIG. 3. (a) Observed spin dynamics after Quench-L sequences at two $t_{\rm ramp}$. Lines are fits based on Eq. (2). Data taken at $t_{\rm ramp} = 1.5$ ms are shifted up by 0.1 for visual clarity. (b) Extracted U_2 and U_2/U_0 from fitting observed dynamics with Eq. (2) at various $t_{\rm ramp}$ [23]. The horizontal line is a linear fit. (c) Similar to panel (b) but based on our data taken under 20 different conditions. The right axis marks the corresponding ratio $a_2/a_0 = (U_2 + U_0)/(U_0 - 2U_2)$, where a_0 and a_2 are scattering lengths.

U_2/U_0 were derived from the scattering lengths [5,27–33]. For example, Refs. [27,28], respectively, found scattering lengths that would lead to $U_2/U_0 = 0.032(14)$ and 0.035(11). In addition, measuring the scattering lengths through Feshbach spectroscopy could yield $U_2/U_0 = 0.037(6)$ [29] and 0.036(3) [30]. Therefore, the observed spin dynamics can conveniently measure spin-dependent interactions and U_2/U_0 with a good resolution.

We also notice one puzzling difference between the nonequilibrium dynamics initiated by Quench-L and Quench-Q sequences: atoms appear to oscillate with a larger amplitude despite having the same frequencies after the Quench-Q sequence, even if spinor gases are prepared into the same final u_L and q by these two quench sequences. This amplitude difference may be attributed to the inevitable dephasing and energy dissipations induced by a number of tunneling processes. Note that atoms are fully localized in individual lattice sites with negligible tunnelings during Quench-Q sequences. In contrast, spinor gases cross SF-MI phase transitions during a Quench-L sequence, tunnelings among adjacent sites thus cannot be ignored during a certain part of this sequence. Other possible reasons for the different oscillation amplitudes may include significant heatings induced by first-order SF-MI phase transitions at a small q during Quench-L sequences [16], different atom number distributions introduced by the quench sequences [34], and nonadiabatic lattice ramps in Quench-L sequences.

To understand how tunnelings affect the spin-mixing dynamics, we monitor spin oscillations after varying the tunneling energy J in a well-controlled way [8]. We first prepare a nonequilibrium initial state with a Quench-Q sequence to $q/h = 30$ Hz in a very deep cubic lattice of $u_{L,x} = u_{L,y} = u_{L,z} = 33(3)E_R$ with $J \simeq 0$, and then suddenly increase J to a desired value by properly reducing only one lattice depth $u_{L,z}$. Here $u_{L,x}$, $u_{L,y}$, and $u_{L,z}$ are depths of the three lattice beams along orthogonal directions, respectively. Results shown in Fig. 4 are collected at four signature $u_{L,z}$, gradually spanning from the few-body dynamics for spinor gases tightly localized in deep lattices at $u_{L,z} = 33E_R$ with $J \simeq 0$, to the many-body dynamics for atoms loosely confined in shallow lattices with $J \gg 0$ at $u_{L,z} = 12E_R$. Amplitudes of spin-mixing oscillations appear to quickly decrease as $u_{L,z}$ is reduced, and completely vanish when $u_{L,z} < 14E_R$. We may understand these observations from two simple illustrations. In one scenario, two atoms oscillate at the frequency f_2 in an $n=2$ lattice site. The spin oscillation disappears as one of the two atoms tunnels out of the site. In another scenario, $n > 2$ atoms oscillate in a lattice site at frequency f_n. After one atom hopping out of this site, spin oscillations occurring in this site and the adjacent site that accepts the atom should be changed. The occurrence of many of such tunneling events could significantly reduce oscillation amplitudes of the observed spin-mixing dynamics. As J increases with the reduction of $u_{L,z}$, the damping is enhanced and

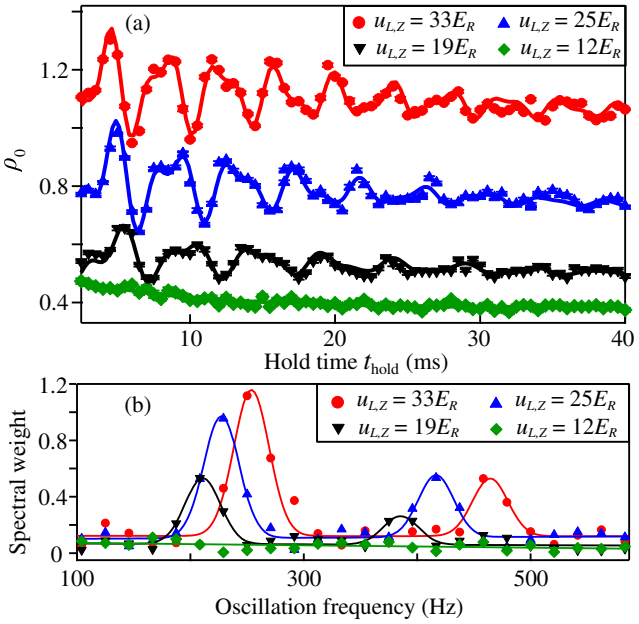

FIG. 4. (a) Observed spin dynamics after Quench-Q sequences to $q/h = 30$ Hz at various $u_{L,z}$ while $u_{L,x} = u_{L,y} = 33(3)E_R$ (see text). Results obtained at $u_{L,z} = 33(3)E_R$, $25(2)E_R$, and $19(2)E_R$ are, respectively, shifted up by 0.55, 0.25, and 0.06 for visual clarity. Lines are fits based on Eq. (2). (b) FFT spectra of the dynamics shown in panel (a). Lines are two-Gaussian fits.

eventually stops the spin oscillations. As a numerical example, the predicted damp time constant due to tunnelings is 11 ms at $u_{L,z} = 19E_R$ [8], which is comparable to the experimental τ_n of around 15 ms extracted from Fig. 4(a). These results justify our use of deep lattices and subsequent neglecting of J in Eq. (1). The underlying physics of the damped spin dynamics and its connection with the Schwinger boson model [35,36] are worthy of further investigation.

Figure 4(b) show the FFT spectra extracted from the nonequilibrium dynamics observed at the four $u_{L,z}$. Each of these FFT spectra has only two distinguished peaks rather than the predicted five peaks; i.e., the wide peaks at around 250 Hz correspond to the oscillations of even n atoms and the wide peaks at around 450 Hz to the oscillations of odd n atoms. One possible reason for this discrepancy is $t_{\rm hold}$ needs to be much longer (greater than 160 ms for all even n) to reduce the aliasing effect of the spectrum analysis, but $t_{\rm hold}$ in our system is limited by lattice heatings and atom losses. The FFT spectra in Fig. 4(b), however, clearly show that a larger $u_{L,z}$ leads to spin oscillations of higher frequencies. This can be interpreted by the fact that frequency f_n is determined by U_2 and thus also by the effective lattice depth $u_L = \sqrt[3]{u_{L,x}u_{L,y}u_{L,z}}$. Our calculations confirm that the effective U_2 gives oscillation frequencies that fall into those broad peaks seen in Fig. 4(b).

In conclusion, we have presented the first experimental study on few-body spin dynamics and transitions between the well-studied two-body and many-body dynamics in

antiferromagnetic spinor BECs. Dynamics consisting of spin-mixing oscillations at multiple frequencies, as opposed to the singular frequency seen in a BEC of thousands of atoms in the superfluid phase, have been observed in time evolutions of the spinor condensate localized in deep lattices after two quench sequences. Unlike the many-body spin dynamics, especially those interpreted by the single mode approximation in Refs. [1–3], the spin-mixing oscillations presented in this Letter indicate quantum recurrences induced by discrete energy spectra [5]. We have confirmed our observed spin-mixing dynamics can reveal atom number distributions of an inhomogeneous system and also enable precise measurements of two key parameters. The lattice quench method is applicable to other spinor systems.

We thank Eite Tiesinga for insightful discussions. We also thank the National Science Foundation, the Noble Foundation, and the Oklahoma Center for the Advancement of Science and Technology for financial support.

*yingmei.liu@okstate.edu

[1] D. M. Stamper-Kurn and M. Ueda, Rev. Mod. Phys. **85**, 1191 (2013).
[2] L. Zhao, J. Jiang, T. Tang, M. Webb, and Y. Liu, Phys. Rev. A **89**, 023608 (2014).
[3] L. Zhao, J. Jiang, T. Tang, M. Webb, and Y. Liu, Phys. Rev. Lett. **114**, 225302 (2015).
[4] C. Becker, P. Soltan-Panahi, J. Kronjäger, S. Dörscher, K. Bongs, and K. Sengstock, New J. Phys. **12**, 065025 (2010).
[5] K. W. Mahmud and E. Tiesinga, Phys. Rev. A **88**, 023602 (2013).
[6] C. B. Dağ, S.-T. Wang, and L.-M. Duan, Phys. Rev. A **97**, 023603 (2018).
[7] M. Lewenstein, A. Sanpera, V. Ahufinger, B. Damski, A. Sen(De), and U. Sen, Adv. Phys. **56**, 243 (2007).
[8] J. S. Krauser, J. Heinze, N. Fläschner, S. Götze, O. Jürgensen, D.-S. Lühmann, C. Becker, and K. Sengstock, Nat. Phys. **8**, 813 (2012).
[9] A. de Paz, A. Sharma, A. Chotia, E. Maréchal, J. H. Huckans, P. Pedri, L. Santos, O. Gorceix, L. Vernac, and B. Laburthe-Tolra, Phys. Rev. Lett. **111**, 185305 (2013).
[10] J. Jiang, L. Zhao, M. Webb, and Y. Liu, Phys. Rev. A **90**, 023610 (2014).
[11] J. Simon, W. S. Bakr, R. Ma, M. E. Tai, P. M. Preiss, and M. Greiner, Nature (London) **472**, 307 (2011).
[12] P. Soltan-Panahi, J. Struck, P. Hauke, A. Bick, W. Plenkers, G. Meineke, C. Becker, P. Windpassinger, M. Lewenstein, and K. Sengstock, Nat. Phys. **7**, 434 (2011).
[13] J. Zeiher, J.-Y. Choi, A. Rubio-Abadal, T. Pohl, R. van Bijnen, I. Bloch, and C. Gross, Phys. Rev. X **7**, 041063 (2017).
[14] A. Widera, F. Gerbier, S. Fölling, T. Gericke, O. Mandel, and I. Bloch, Phys. Rev. Lett. **95**, 190405 (2005).
[15] A. Widera, F. Gerbier, S. Fölling, T. Gericke, O. Mandel, and I. Bloch, New J. Phys. **8**, 152 (2006).
[16] J. Jiang, L. Zhao, S.-T. Wang, Z. Chen, T. Tang, L.-M. Duan, and Y. Liu, Phys. Rev. A **93**, 063607 (2016), and the references therein.
[17] L. Zhao, T. Tang, Z. Chen, and Y. Liu, arXiv:1801.00773.
[18] See Supplemental Material at http://link.aps.org/supplemental/10.1103/PhysRevLett.123.113002 for additional details of our experimental procedures and analysis methods.
[19] N. T. Phuc, Y. Kawaguchi, and M. Ueda, Phys. Rev. A **84**, 043645 (2011).
[20] Our calculations based on Eq. (1) indicate spin oscillation amplitudes D_n for an inhomogeneous system with $n_{\mathrm{peak}} = 6$ at $q/h = 85$ Hz are $D_1 = 0$, $D_2 = 0.413$, $D_3 = 0.229$, $D_4 = 0.269$, $D_5 = 0.215$, and $D_6 = 0.199$. Because no spin oscillations occur when $n = 1$, χ_n shown in Fig. 2 reflect the normalized number distributions after the $n = 1$ Mott lobe is excluded.
[21] When $t_{\mathrm{ramp}} < 1$ ms, we find atoms in our system need an additional 1 ms to completely lose their phase coherence. A similar phenomenon has also been reported in rubidium systems [22].
[22] J. Sebby-Strabley, B. L. Brown, M. Anderlini, P. J. Lee, W. D. Phillips, J. V. Porto, and P. R. Johnson, Phys. Rev. Lett. **98**, 200405 (2007).
[23] U_0 is derived from Ref. [24].
[24] D. Jaksch, C. Bruder, J. I. Cirac, C. W. Gardiner, and P. Zoller, Phys. Rev. Lett. **81**, 3108 (1998).
[25] T. L. Ho, Phys. Rev. Lett. **81**, 742 (1998).
[26] T. Ohmi and K. Machida, J. Phys. Soc. Jpn. **67**, 1822 (1998).
[27] A. Crubellier, O. Dulieu, F. Masnou-Seeuws, M. Elbs, H. Knöckel, and E. Tiemann, Eur. Phys. J. D **6**, 211 (1999).
[28] F. A. van Abeelen and B. J. Verhaar, Phys. Rev. A **59**, 578 (1999).
[29] C. Samuelis, E. Tiesinga, T. Laue, M. Elbs, H. Knöckel, and E. Tiemann, Phys. Rev. A **63**, 012710 (2000).
[30] S. Knoop, T. Schuster, R. Scelle, A. Trautmann, J. Appmeier, M. K. Oberthaler, E. Tiesinga, and E. Tiemann, Phys. Rev. A **83**, 042704 (2011).
[31] K. Fujimoto and M. Tsubota, Phys. Rev. A **88**, 063628 (2013).
[32] J. Lovegrove, M. O. Borgh, and J. Ruostekoski, Phys. Rev. Lett. **112**, 075301 (2014).
[33] S. Yi and H. Pu, Phys. Rev. Lett. **97**, 020401 (2006).
[34] Z. Chen, J. Austin, Z. Shaw, L. Zhao, and Y. Liu (to be published).
[35] E. Altman and A. Auerbach, Phys. Rev. Lett. **89**, 250404 (2002).
[36] S. M. Davidson and A. Polkovnikov, Phys. Rev. Lett. **114**, 045701 (2015).

Supplemental Material: Quantum quench and non-equilibrium dynamics in lattice-confined spinor condensates

Z. Chen, T. Tang, J. Austin, Z. Shaw, L. Zhao, and Y. Liu

Department of Physics, Oklahoma State University, Stillwater, Oklahoma 74078, USA

(Dated: August 3, 2019)

I. EXPERIMENTAL PROCEDURES

Figure S1 illustrates two experimental sequences, Quench-L and Quench-Q sequences, used in this paper. Each sequence starts in free space at $q/h = 40$Hz with a spin-1 antiferromagnetic spinor Bose-Einstein condensate (BEC) of up to 10^5 sodium (^{23}Na) atoms in its ground state, the longitudinal polar (LP) state with $\rho_0 = 1$ and $m = 0$. Similar to our previous work, we prepare the LP state by eliminating all $|F = 1, m_F = \pm 1\rangle$ atoms with resonant microwave and laser pulses [1, 2]. Atoms in the LP state are then loaded at a given q into a cubic lattice constructed by three standing waves along orthogonal directions. The lattice spacing is 532 nm, while lattice beams are originated from a single-mode laser at 1064 nm and frequency-shifted by at least 20 MHz with respect to each other. We calibrate the lattice depth u_L with Kapitza-Dirac diffraction patterns. In a Quench-L sequence, the lattice ramp time $t_{\rm ramp}$ is carefully chosen based on the following two criteria. First, $t_{\rm ramp}$ is long enough to satisfy the interband adiabaticity requirement $du_L/dt \ll 32\pi E_R^2/h$ [2]. Second, $t_{\rm ramp}$ is short enough to initiate spin-mixing oscillations, while sufficiently long to limit the oscillations between the ground states and the first excited states. After being prepared into desired q and u_L via a Quench-L or a Quench-Q sequence, the atoms are held in the lattices for a certain time $t_{\rm hold}$. We then abruptly release the atoms from the lattices, and measure ρ_0 with Stern-Gerlach absorption imaging and our two-step microwave imaging after a given time of flight [2]. Each value of ρ_0 presented in this paper is extracted from averaging approximately 15 repeated measurements. All quoted uncertainties of ρ_0 are estimated one standard error.

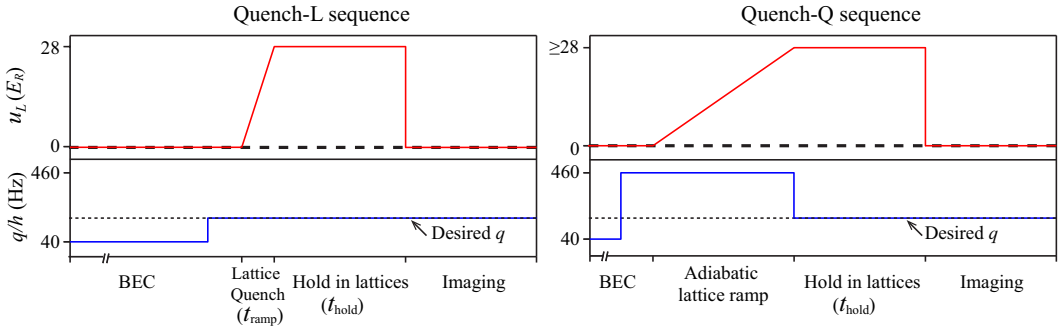

FIG. S1. Schematic of our Quench-L and Quench-Q sequences (see text). All axes are not to scale.

II. FITTING METHODS

We find all observed spin dynamics can be fit by the empirical model, Eq. 2, as explained in the main text. For improving and simplifying the fittings, we keep the damp time constants τ_n at fixed values. Figure S2 uses the $q/h = 85$ Hz data set shown in Fig. 1(a) to illustrate how we can extract τ_n from a series of FFT spectra. We first conduct Fourier transformations onto the $q/h = 85$ Hz data set over various time regions, starting at $t_{\rm hold}^{\rm start}$ and ending

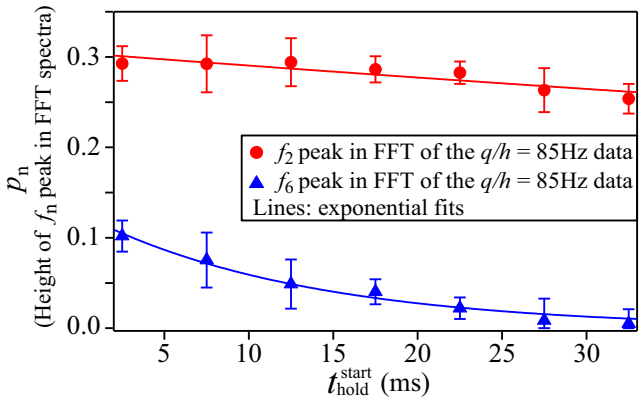

FIG. S2. Circles (triangles) represent p_2 (p_6) as a function of $t_{\rm hold}^{\rm start}$. Here p_n is the height of the peak centered at f_n in a FFT spectrum of the $q/h = 85$ Hz data set shown in Fig. 1(a), and each FFT starts at $t_{\rm hold}^{\rm start}$ (see text). Lines are exponential fits.

at $t_{\rm hold}^{\rm end} = t_{\rm hold}^{\rm start} + 40$ ms. The obtained FFT spectra at this q are similar to those shown in Fig. 2(a), i.e., each has five distinguished peaks agreeing well with the predictions of Eq. 1. We plot p_n, the height of the peak centered at oscillation frequency f_n in a FFT spectrum, as a function of $t_{\rm hold}^{\rm start}$ for each fixed n. Two typical examples are shown in Fig. S2. The apparent decays of p_n with $t_{\rm hold}^{\rm start}$ reflect the damping of the spin-mixing oscillations. The damp time constant τ_n can thus be extracted from an exponential fit to the data at a fixed n, as shown by solid lines in Fig. S2. During the fittings of the spin dynamics for the $q/h = 85$ Hz data, τ_n are fixed at these extracted values, as exemplified in Table S1.

Fixed parameters:

τ_2 (ms)	τ_3(ms)	τ_4(ms)	τ_5(ms)	τ_6 (ms)
214	30	34	12	13

Fitting parameters:

U_2/h (Hz)	A_2	A_3	A_4	A_5	A_6	t_0 (ms)	τ_0 (ms)	$\Delta\rho_0$
79.4	0.017	0.012	0.02	0.012	0.01	0.48	87-0.34$t_{\rm hold}$	0.472

TABLE S1. Parameters used in the blue solid line in Fig. 1(a) (see text).

Table S1 also lists the fitting parameters used in a good fitting curve for the $q/h = 85$ Hz data based on Eq. 2, as displayed by the blue solid line in Fig. 1(a). In this fit, the decay constant τ_0 reduces with hold time, indicating the spin oscillation decays more quickly due to more induced heatings at longer $t_{\rm hold}$. The best fits for other data sets taken at smaller q, however, all yield constant τ_0. The underlying physics of this field-dependent heating requires further study. We can also deduce atom number distributions χ_n from dividing the fitting parameters A_n listed in Table S1 by the spin oscillation amplitude D_n (see Ref. 19 in the main text). Agreements are found between these deduced χ_n and the results shown in Fig. 2(b). In addition, the value of $\Delta\rho_0$ in Table S1 confirms that $\Delta\rho_0 + 1/3 \approx \rho_0^T$, where ρ_0^T is the predicted ρ_0 in the ground state of the spinor gases at the given q and u_L based on Eq. 1 and the Thomas-Fermi approximation.

[1] J. Jiang, L. Zhao, S.-T. Wang, Z. Chen, T. Tang, L.-M. Duan, and Y. Liu, Phys. Rev. A **93**, 063607 (2016).

[2] L. Zhao, T. Tang, Z. Chen, and Y. Liu, arXiv:1801.00773 (2018).